



Green, K., & Krauskopf, B. (2002). *Bifurcation analysis of frequency locking in a semiconductor laser with phase-conjugate feedback*.
<http://hdl.handle.net/1983/481>

Early version, also known as pre-print

[Link to publication record in Explore Bristol Research](#)
PDF-document

University of Bristol - Explore Bristol Research

General rights

This document is made available in accordance with publisher policies. Please cite only the published version using the reference above. Full terms of use are available:
<http://www.bristol.ac.uk/red/research-policy/pure/user-guides/ebr-terms/>

Bifurcation analysis of frequency locking in a semiconductor laser with phase-conjugate feedback

Kirk Green^{*} and Bernd Krauskopf[†]

Department of Engineering Mathematics, University of Bristol,
Bristol BS8 1TR, UK

May 2002

Abstract

We present a detailed study of the external-cavity modes (ECMs) of a semiconductor laser with phase-conjugate feedback. Mathematically, lasers with feedback are modelled by delay differential equations (DDEs) with an infinite dimensional phase space. We employ new numerical bifurcation tools for DDEs to continue steady states and periodic orbits, irrespective of their stability. In this way, we show that the periodic orbits corresponding to the ECMs are connected to the steady state solution associated with the locking range of the laser. We also identify symmetric and non-symmetric homoclinic orbits and hysteresis in the system.

1 Introduction

Delay differential equations (DDEs) [Diekmann et. al. 1995, Hale and Verduyn Lunel 1993] have received a lot of attention recently in the modelling of dynamical systems where a feedback term is present. Examples of fields in which DDEs are used to model a feedback term include, biology [Murray 1980], chemistry [Epstein and Pojman 1998] and neuroscience [Longtin et. al. 1990]. In particular, DDEs are used to model semiconductor lasers subject to delayed optical feedback, such as lasers with conventional optical feedback (COF) from an external mirror, lasers with optoelectronic feedback, mutually coupled lasers with delay, and lasers with phase-conjugate feedback (PCF), the case considered here. These types of feedback lasers have been studied extensively over the last decade by

^{*}Email: kirk.green@bristol.ac.uk

[†]Email: b.krauskopf@bristol.ac.uk

techniques involving the computation of bifurcation diagrams, phase portraits and optical spectra, obtained by numerical simulation of the governing DDEs; see, for example, [Van Tartwijk and Agrawal 1998], [Krauskopf and Lenstra 2000] and further references therein. However, it has only recently become possible to perform detailed numerical bifurcation analysis by continuation methods for DDEs with the release of the package DDE-BIFTOOL [Engelborghs 2000]. It allows numerical continuation of steady states and periodic solutions in systems of DDEs, irrespective of their stability, and also detects local bifurcations. In the series of papers, [Pieroux, Erneux, Haegeman, Engelborghs and Roose 2001, Pieroux, Erneux, Luzyanina and Engelborghs 2001, Haegeman et. al. 2002], connecting bridges of periodic solutions were studied between steady states in the COF laser using DDE-BIFTOOL. Similar work on the rate equations describing a vertical-cavity surface-emitting laser (VCSEL) can be found in [Sciamanna et. al. 2002]. Continuation studies of the PCF laser can be found in [Green and Krauskopf 2001]. Furthermore, in [Krauskopf and Green 2002] we developed a method to calculate unstable manifolds of periodic orbits in DDEs, which was used in combination with DDE-BIFTOOL in [Green et. al. 2002] to study the break-up of a torus in the PCF laser.

In this paper, we use these new continuation techniques to study a semiconductor laser receiving (instantaneous) phase-conjugate feedback (PCF) from a phase-conjugating mirror (PCM) [Agrawal and Gray 1992, Gray et. al. 1994, Krauskopf et. al. 1998, Van Tartwijk et. al. 1995]. Phase-conjugate feedback is very desirable as it produces a return wave that coincides exactly with the incident wave. In other words, the system is self-aligning. However, PCF is experimentally difficult to achieve, but can be generated by degenerate four-wave mixing, a nonlinear process involving counter propagating laser beams in an atomic vapour or a semiconductor material [Breton et. al. 1991, Shimura et. al. 1993]. The PCF laser is shown schematically in Fig. 1. The length of the laser is typically of order 0.1 mm, while the length of the external cavity can be a few centimetres to one metre. This leads to a large delay relative to the time-scale of the semiconductor laser.

More specifically, we perform a detailed bifurcation analysis of periodic orbits found in the PCF laser. In a bifurcation diagram obtained by simulation one finds stable periodic orbits interspersed with bubbles of more complicated dynamics, which for the most part are chaotic; see already Fig. 2. Between these bubbles the PCF laser is frequency locked, with its intensity oscillating close to some integer multiple of the fundamental external-cavity frequency [Krauskopf et. al. 1998]. One therefore refers to these stable periodic orbits as external-cavity modes (ECMs) of the PCF laser. We remark that one also finds external-cavity modes in the COF laser, in which they are also referred to as continuous wave (CW) states. In the COF laser, a CW-state is a periodic solution with constant intensity and inversion, and a linearly evolving phase, of which solutions can be found analyti-

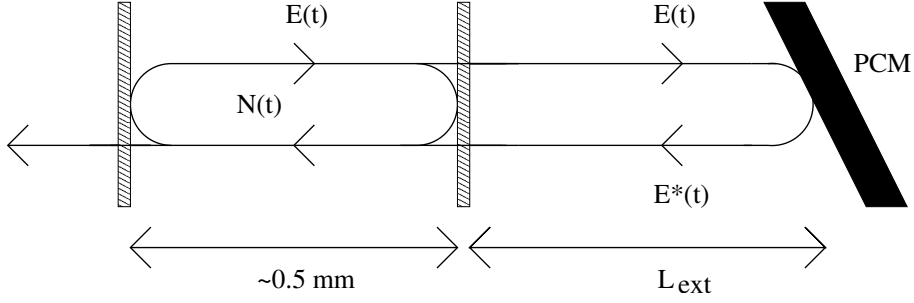


Figure 1: Sketch of a semiconductor laser with phase-conjugate feedback.

cally [Van Tartwijk and Agrawal 1998, Verduyn Lunel and Krauskopf 2000]. We remark that this nature of the CW-states is a consequence of the S^1 -symmetry of the COF laser. (Mathematically, the CW-states of the COF laser are group orbits of a steady state under the S^1 -symmetry [Krauskopf et. al. 2000].) In contrast, the ECMs of the PCF laser are genuine periodic orbits with a periodically evolving intensity and inversion, and therefore cannot be found analytically. Hence the need to employ advanced numerical tools to investigate them.

Our main tool is DDE-BIFTOOL, which we use to continue the branches of symmetric periodic orbits on which each ECM lies. By detecting symmetry-breaking bifurcations along these symmetric branches we can switch to and continue branches of non-symmetric periodic orbits. In fact, DDE-BIFTOOL was extended to allow branch switching at symmetry-breaking bifurcations to allow investigation of the PCF laser [Green et. al. 2002]. Continuation of these non-symmetric branches shows that a number of them end in Hopf bifurcations. Therefore, an immediate question is, are all ECMs of the PCF laser connected to one another via a non-symmetric steady state?

We answer this question to the positive, by giving a complete view of the ECMs and their bifurcating branches and show how they are connected. This includes identifying symmetric and non-symmetric branches, and all local bifurcations along those branches. We also identify homoclinic bifurcations of symmetric and non-symmetric periodic solutions, extra regions of stability and a bistability which leads to a hysteresis loop.

| parameter | value |
|-----------|-------------------------|
| α | 3.0 |
| G_N | 1190 s ⁻¹ |
| τ_p | 1.4 ps |
| I | 65.1 mA |
| q | 1.6×10^{-19} C |
| τ_e | 2.0 ns |
| N_0 | 1.64×10^8 |

Table 1: Parameter values.

2 Rate equations

The rate equations describing the PCF laser are well established [Agrawal and Gray 1992, Gray et. al. 1994] and can be written as

$$\begin{aligned} \frac{dE(t)}{dt} = \frac{1}{2} \left[-i\alpha G_N(N(t) - N_{\text{sol}}) + \left(G(t) - \frac{1}{\tau_p} \right) \right] E(t) \\ + \kappa E^*(t - \tau) \exp[i\phi_{\text{PCM}}] \end{aligned} \quad (1)$$

$$\frac{dN(t)}{dt} = \frac{I}{q} - \frac{N(t)}{\tau_e} - G(t) |E(t)|^2$$

for the evolution of the slowly varying complex electric field $E(t) = E_x(t) + iE_y(t)$ and the population inversion $N(t)$. In system (1), nonlinear gain is included as $G = G_N(N - N_0)(1 - \epsilon P)$, where $\epsilon = 3.57 \times 10^{-8}$ is the nonlinear gain coefficient and $P = |E(t)|^2$ is the intensity of the electric field. This produces an effective detuning of 166 MHz. Parameter values are set to the realistic values [Gray et. al. 1994, Krauskopf et. al. 1998] shown in Table 1. The phase shift ϕ_{PCM} at the PCM was set to zero and $N_{\text{sol}} = N_0 + 1/(G_N\tau_p)$. The feedback term in system (1) involves the feedback rate κ and the external cavity round-trip time $\tau = 2L_{\text{ext}}/c$ which we fix at $\tau = 2/3$ ns, corresponding to an external cavity length of $L_{\text{ext}} \approx 10$ cm. Together they form the dimensionless bifurcation parameter $\kappa\tau$.

Mathematically, system (1) is a delay differential equation (DDE). The state of the system at time $t > 0$ is a continuous function on the time interval $[t - \tau, t]$, which is an evolution of the initial condition defined on the time interval $[-\tau, 0]$ [Diekmann et. al. 1995, Hale and Verduyn Lunel 1993, Verduyn Lunel and Krauskopf 2000]. Therefore, the system is infinite-dimensional. While (E, N) -space is not the phase space of system (1), it is nevertheless helpful to show the dynamics projected onto (E, N) -space, which is also called the physical space of system (1).

System (1) has \mathbb{Z}_2 -symmetry under the transformation $E \rightarrow -E$, which

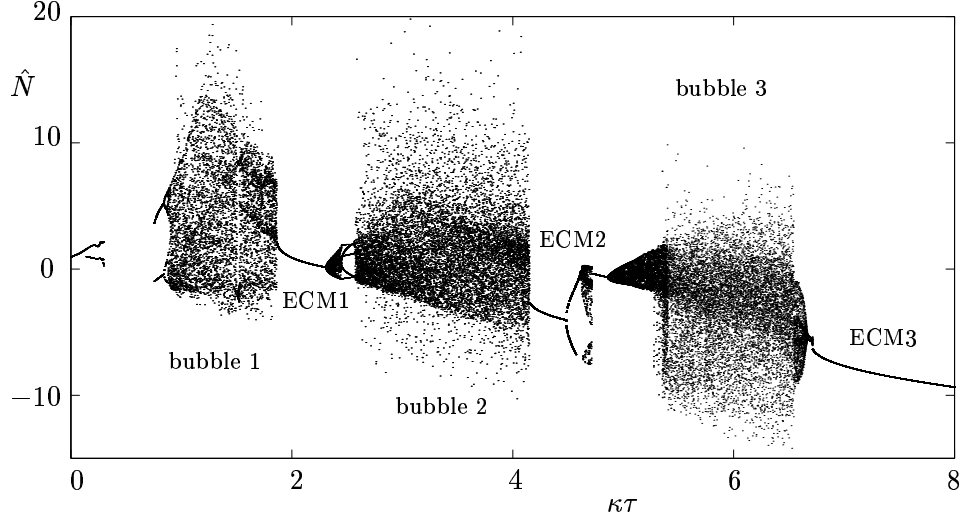


Figure 2: Bifurcation diagram obtained by simulation showing normalized inversion \hat{N} versus the feedback strength $\kappa\tau$. The stable periodic orbits corresponding to ECM1, ECM2 and ECM3 are interspersed with three bubbles of chaotic dynamics.

corresponds to a rotation over π of the complex E -plane, so that an attractor is either symmetric, or has a symmetric counterpart [Krauskopf et. al. 1998, Krauskopf et. al. 2000]. Physically, this symmetry corresponds to a phase shift by π of the laser light. The symmetry implies restrictions on the types of bifurcations of periodic orbits: for example, symmetric periodic orbits cannot undergo period-doubling bifurcations [Kuznetsov 1995]. More generally, this discrete symmetry allows for the possibility of symmetry-breaking bifurcations.

Figure 2 shows a bifurcation diagram obtained by simulation. It gives a first impression of the dynamics and bifurcations of the PCF laser as the feedback parameter $\kappa\tau$ is increased. For each value of $\kappa\tau$ we numerically integrated system (1), using an initial condition from the attractor corresponding to the previous value of $\kappa\tau$ (thus, for non-symmetric solutions assuring that we did not switch between symmetric counterparts). We then plotted the normalized value of the inversion $\hat{N} = (N/N_{\text{sol}} - 1) \times 10^3$ whenever the intensity P crossed its average value in the increasing direction [Green et. al. 2002, Krauskopf et. al. 1998]. The region with no points corresponds to a steady state. A small number of points correspond to a periodic orbit. While a large number of points correspond to quasiperiodic or chaotic dynamics.

In Fig. 2 the stable periodic orbits corresponding to the ECMs can clearly be seen interspersed with the bubbles of chaotic dynamics. Within these bubbles of chaos the laser is between ECMs. The complex dynamics can be thought of as the result of a competition between ECMs.

We observe an absence of points for $\kappa\tau \in [0.279, 0.749]$ corresponding to an attracting steady state. Physically, this corresponds to a frequency match between the PCM pump laser and the solitary laser. Here the laser frequency and phase are locked. The laser phase no longer undergoes diffusion and, subsequently, the line-width of the laser is extremely narrow [Agrawal and Gray 1992, Van Tartwijk et. al. 1995]. This narrow line-width was shown to remain stable even with the addition of noise from spontaneous emission [Gray et. al. 1994]. This is why the PCF laser is interesting for applications requiring narrow laser line-width, such as, spectroscopy. We will see in Sec. 3 that this locked state is the non-symmetric steady state to which the branches of periodic orbits associated with each ECM are connected.

3 Bifurcation analysis

In order to provide a complete picture of the dynamics and bifurcations of system (1) one must look beyond simulation. We now show that a bifurcation analysis of periodic orbits, where we start from the stable periodic orbits observed in Fig. 2, is needed to give a full explanation of the ECMs of the PCF laser.

3.1 Bifurcations and Continuation

The continuation package DDE-BIFTOOL [Engelborghs 2000] allows computation of branches of steady states and periodic solutions irrespective of their stability. For steady states, it approximates the right most roots of the characteristic equation and corrects them using Newton iteration. Furthermore, orthogonal collocation based on a piecewise polynomial representation with an adaptive mesh is used to compute periodic solutions and approximations of the associated Floquet multipliers. This is similar to the technique used in the package AUTO [Doedel et. al. 1997] to approximate the solutions to boundary value problems for ordinary differential equations (ODEs).

Although DDE-BIFTOOL supports no automatic detection of bifurcations at present, the eigenvalues or Floquet multipliers along a branch of solutions can be tracked using appropriate visualisation and, thus, local bifurcations can be detected. When a real Floquet multiplier passes through the unit circle at +1 there are two possible bifurcations. The first is a *saddle-node bifurcation of limit cycles*. Here a saddle periodic orbit collides with a stable periodic orbit (or another saddle periodic orbit) and both are destroyed, the solution then jumps to a different attractor. The second

possible bifurcation, due to the \mathbb{Z}_2 -symmetry of system (1), is a *symmetry-breaking bifurcation*. Here the symmetric periodic orbit is split into two non-symmetric periodic orbits which are initially almost symmetric but lose symmetry as one moves away from the bifurcation point. In bifurcation diagrams obtained by simulation a symmetry-breaking bifurcation shows up as a doubling in the number of intersection points, for example, see Fig. 2 at $\kappa\tau \approx 4.5$. Experimentally, this is identified by a doubling in the period of the power. Therefore, one must be careful not to confuse a symmetry-breaking bifurcation with a *period-doubling bifurcation* which occurs when a real Floquet multiplier passes through the unit circle at -1 ; only non-symmetric solutions can undergo period-doubling [Kuznetsov 1995]. Lastly, when a pair of complex conjugate Floquet multipliers pass through the unit circle a *torus* (or Neimark-Sacker) *bifurcation* takes place.

3.2 Continuation of the steady state

Figure 3 (a) shows continuation of the non-symmetric steady state, where we started from the stable (locked) state in Fig. 2. When the steady state is stable it is denoted by a thick curve and by a thin curve otherwise. The steady state is created at $\kappa\tau \approx 0.279$ in a saddle-node bifurcation. It is destabilized in a sub-critical Hopf bifurcation H_1 at $\kappa\tau \approx 0.749$. We also identify further Hopf bifurcations H_2 to H_6 when the steady state is already unstable, which we refer to later in Sec. 3.3. For a detailed discussion of this steady state we refer to [Green and Krauskopf 2001]. Here, we concentrate on the branches and bifurcations of periodic orbits associated with the ECMs.

3.3 Continuation of ECMs

Figures 3 (b) and 4 were obtained by continuation with DDE-BIFTOOL of the periodic orbits associated with each ECM. They show branches of periodic orbits, denoted by thick curves when stable, and by thin curves otherwise. In order to directly compare a periodic solution with a steady state in Fig. 3 (b) we plot a normalized amplitude $|\max(\text{Re}(E)) - \min(\text{Re}(E))|$ against $\kappa\tau$. This plot may appear complicated, but continuation of bifurcating (non-symmetric) branches clearly show that a number of them end in Hopf bifurcations, identified by a normalized amplitude of zero. Indeed, they end at the Hopf bifurcation points $H_{1,2,3,6}$ already indicated in Fig. 3 (a). This provides a connection between the different ECMs. The different branches corresponding to each ECM are further distinguished by the frequency ranges, as is highlighted in Fig. 4, where they are plotted as a function of their period T . In both figures, all branches associated with the first, second and third external-cavity modes (ECM1–ECM3) are blue, green and red, respectively. The interval of $\kappa\tau \in [0, 8]$ was chosen to contain

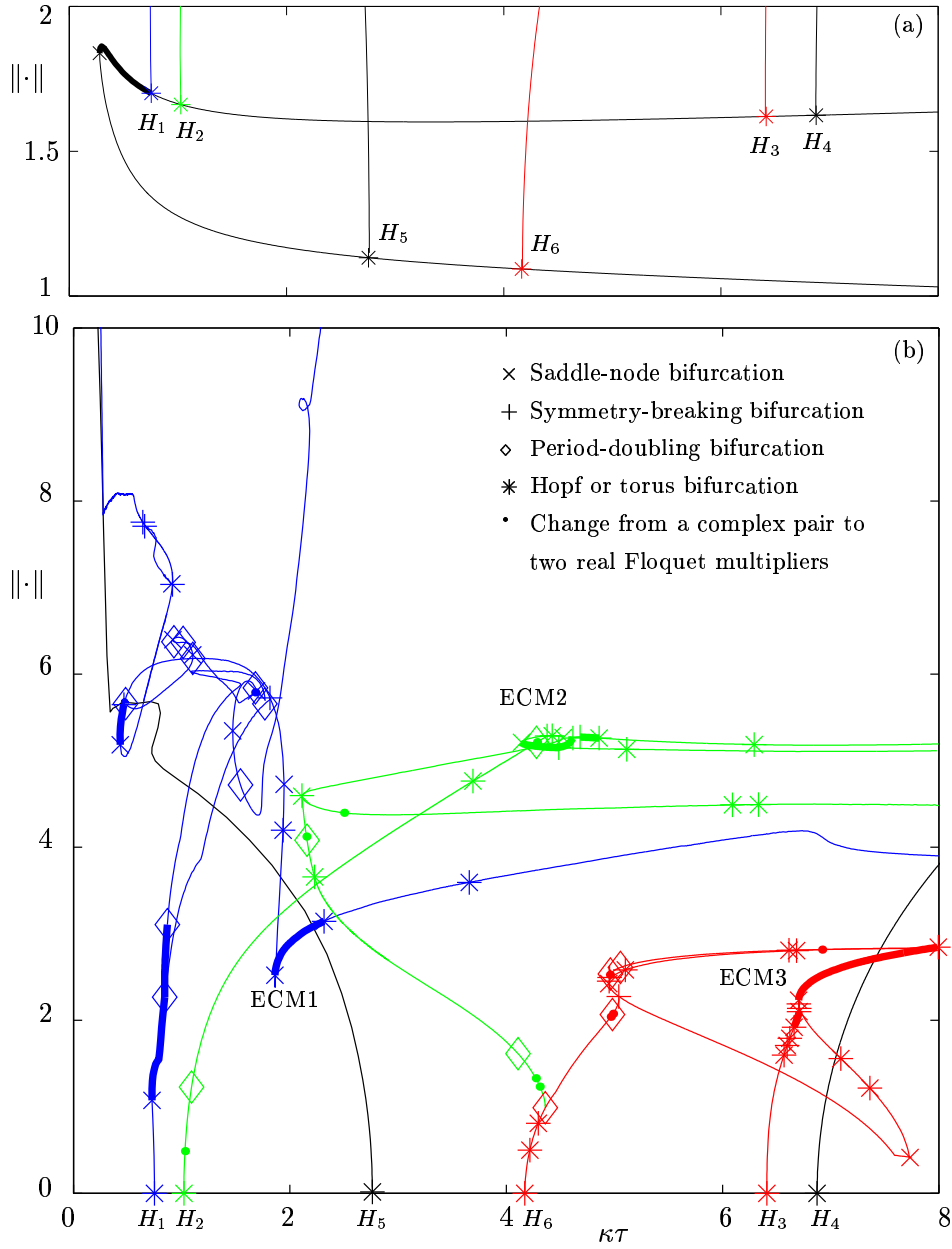


Figure 3: Bifurcation diagrams computed with DDE-BIFTOOL showing a normalized amplitude versus $\kappa\tau$ for the steady states (a) and for all branches emanating from the external-cavity modes (b).

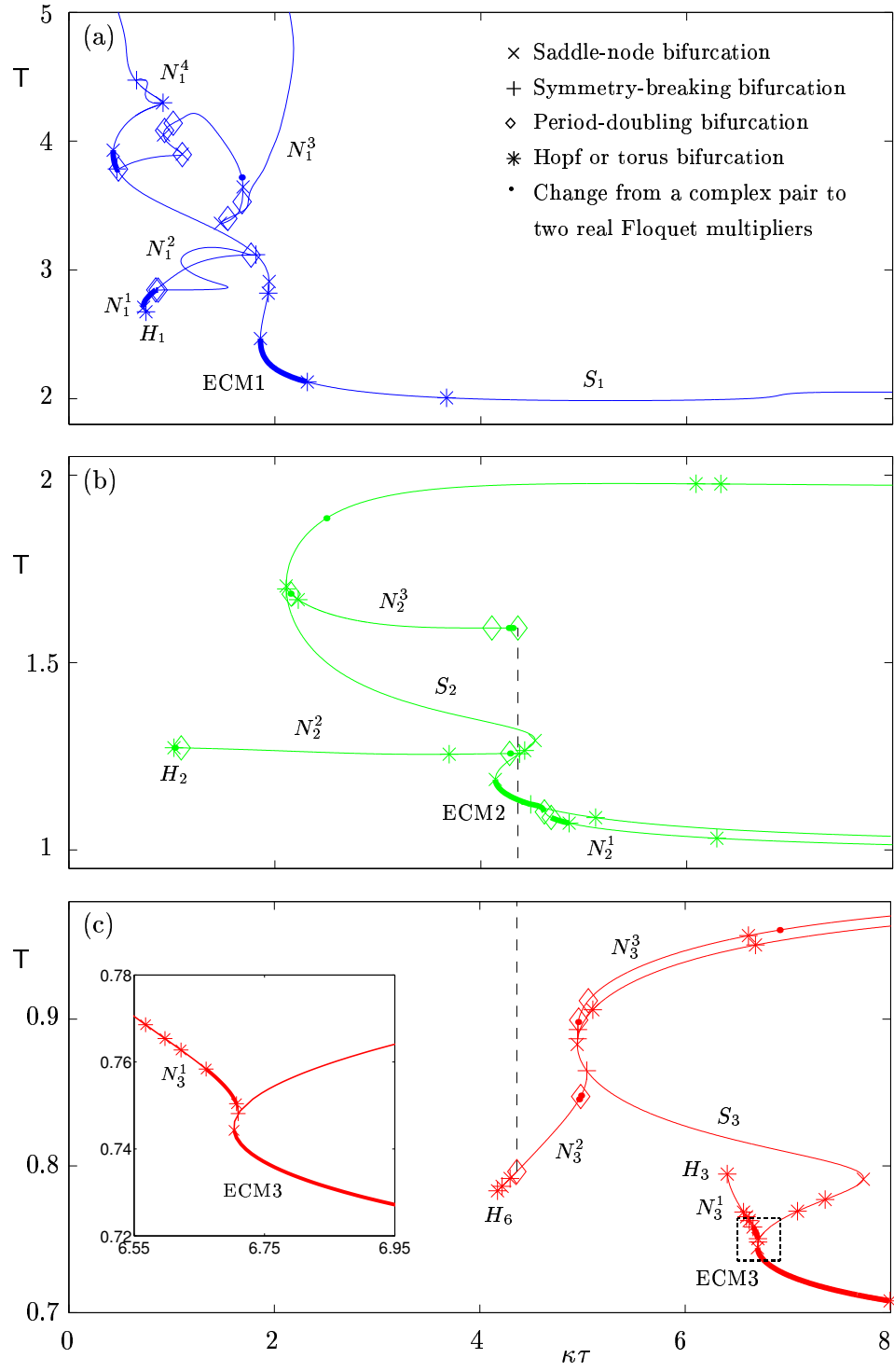


Figure 4: Bifurcation diagrams as in Fig. 3 (b), but plotted as period T versus $\kappa\tau$.

the first three ECMs.

The main branches, on which the ECMs lie are of symmetric periodic orbits and, therefore, since symmetric periodic orbits can not undergo period-doubling bifurcations [Kuznetsov 1995], all branches of periodic orbits which bifurcate from this main symmetric branch are non-symmetric. Another consequence of the \mathbb{Z}_2 -symmetry is that for a symmetric periodic orbit the intensity is periodic with period $T/2$, while the period of the corresponding periodic orbit is T [Krauskopf et. al. 2000]. With this in mind, we see that ECM1 has a period ranging from 2.13τ s to 2.47τ s; ECM2 from 1.12τ s to 1.19τ s; and ECM3 from 0.71τ s to 0.74τ s, corresponding to frequency ranges of 1.21 GHz to 1.40 GHz; 2.51 GHz to 2.67 GHz; and 4.03 GHz to 4.20 GHz, respectively. This agrees well with the frequencies of 1.5 GHz, 3.0 GHz and 4.5 GHz mentioned in [Krauskopf et. al. 1998].

We computed the branches of periodic orbits which end at the Hopf points $H_{1,2,3,6}$ by starting from an ECM and continuing branches of periodic orbits. The two branches of periodic orbits emanating from H_3 and H_4 in Fig. 3 (a) are not directly related to the ECMs we considered and were computed from the periodic orbits created at the Hopf points. The branch emanating from H_3 leads to a branch of unstable periodic orbits which ends in a homoclinic bifurcation; see Sec. 3.5. We note that this branch is not connected to any of the symmetric branches on which the ECMs lie. The branch emanating from H_4 is connected to the symmetric branch on which the fourth ECM lies, which is beyond the scope of this paper.

Notice that when plotted as a function of the period T , as in Fig. 4, the symmetric branches (on which the ECMs lie) have a similar shape. In each case, a lower part of the curve contains the ECM (thick curve) is destabilized when decreasing $\kappa\tau$, in a saddle-node bifurcation of limit cycles; see also Sec. 3.4.

Figure 3 (b) clearly shows that bifurcating branches emanating from the main branches on which the ECMs lie end in Hopf bifurcations associated with the same non-symmetric steady state; identified in Figs. 2 and 3 (a). In order to provide a complete picture of these connections, these bifurcation diagrams should be looked at together with the phase portraits along them, shown in Figs. 5, 6 and 7, which we now discuss in some detail.

3.4 Bifurcations along branches

Figure 5 shows periodic orbits along the blue branch associated with ECM1. Along the symmetric branch S_1 (see panels (a1) to (a8)) the unstable periodic orbit, shown in panel (a1), is stabilized in a torus bifurcation at $\kappa\tau \approx 2.307$ as $\kappa\tau$ is decreased. The ensuing stable periodic orbit (see panel (a2)) is ECM1. It is destabilized in a saddle-node bifurcation of limit cycles at $\kappa\tau \approx 1.860$, where, as Fig. 2 shows, the attracting solution becomes chaotic. Continuing S_1 further, one sees the branch pass through a number

of bifurcations before a symmetry-breaking bifurcation at $\kappa\tau \approx 0.471$ again stabilizes the branch. The ensuing stable periodic orbit, shown in panel (a4), is not seen by simulation in Fig. 2 as it is connected to the main attractor of the system by branches of unstable solutions. A saddle-node bifurcation of limit cycles destabilizes this periodic orbit at $\kappa\tau \approx 0.430$. Its period then starts to grow rapidly, and the periodic orbit spirals around the origin of the E -plane, this is shown in panels (a5) to (a7). This is evidence that the periodic orbit is approaching a homoclinic bifurcation. We detail this in Sec. 3.5.

Figures 5 (b1)–(b4) and (c1)–(c4) show non-symmetric periodic orbits along branches N_1^1 and N_1^2 , respectively. Along N_1^1 , we see a clear change in symmetry as the branch extends from the symmetry-breaking bifurcation point on S_1 at $\kappa\tau \approx 1.822$. Initially the periodic orbit, shown in panel (b1), is almost symmetric but quickly loses symmetry, before shrinking about the non-symmetric steady state (see panel (b4)) associated with the Hopf bifurcation H_1 . This change in symmetry can also be seen along the period-two branch N_1^2 , which bifurcates from N_1^1 at $\kappa\tau \approx 0.843$ (marking the start of the period doubling cascade shown in Fig. 2) and rejoins N_1^1 close to the symmetric branch S_1 at $\kappa\tau \approx 1.770$. The period-two orbits in panels (c1) to (c4) should be directly compared to the period-one orbits in panels (b1) to (b3).

The phase portraits along the non-symmetric branch N_1^3 are given in Fig. 5 (d1) to (d8). The branch N_1^3 bifurcates from S_1 at the symmetry-breaking bifurcation at $\kappa\tau \approx 0.471$. Again, the initial stable periodic orbit, shown in panel (d1), is almost symmetric. It should be compared with the symmetric periodic orbit in panel (a4). However, stability is quickly lost in a period-doubling bifurcation. The ensuing unstable periodic orbits in panels (d2) to (d8) quickly lose symmetry. They increasingly look like ‘one half’ of the symmetric periodic orbits of panels (a5) to (a8). As one moves along N_1^3 , one ‘arm’ of the periodic orbit retracts about the origin of the E -plane. However, an image of the larger arm along with its symmetric counterpart is directly comparable with the symmetric orbits along S_1 . Finally, as with S_1 (see panel (a8)), N_1^3 ends in a homoclinic bifurcation. An example of this non-symmetric homoclinic orbit, which we investigate in detail in Sec. 3.5, is shown in panel (d8).

Periodic orbits associated with ECM2 and ECM3 are shown in Figs. 6 and 7. The symmetric periodic orbits along S_2 and S_3 are shown in Figs. 6 (a1)–(a4) and 7 (a1)–(a4), respectively. In both cases, no qualitative change in the shape of the orbits is observed. Figures 6 (b1)–(b4), 7 (b1)–(b4) and 7 (c1)–(c4) show how bifurcating non-symmetric branches N_2^2 , N_3^1 and N_3^2 end at the Hopf bifurcations H_2 , H_3 and H_6 . As in the case of branch N_1^1 , in all cases, the periodic orbit is seen to lose symmetry as one moves from the bifurcation point, before shrinking about the non-symmetric steady state associated with the respective Hopf bifurcation.

Apart from the Hopf bifurcations associated with ECM2 and ECM3 we

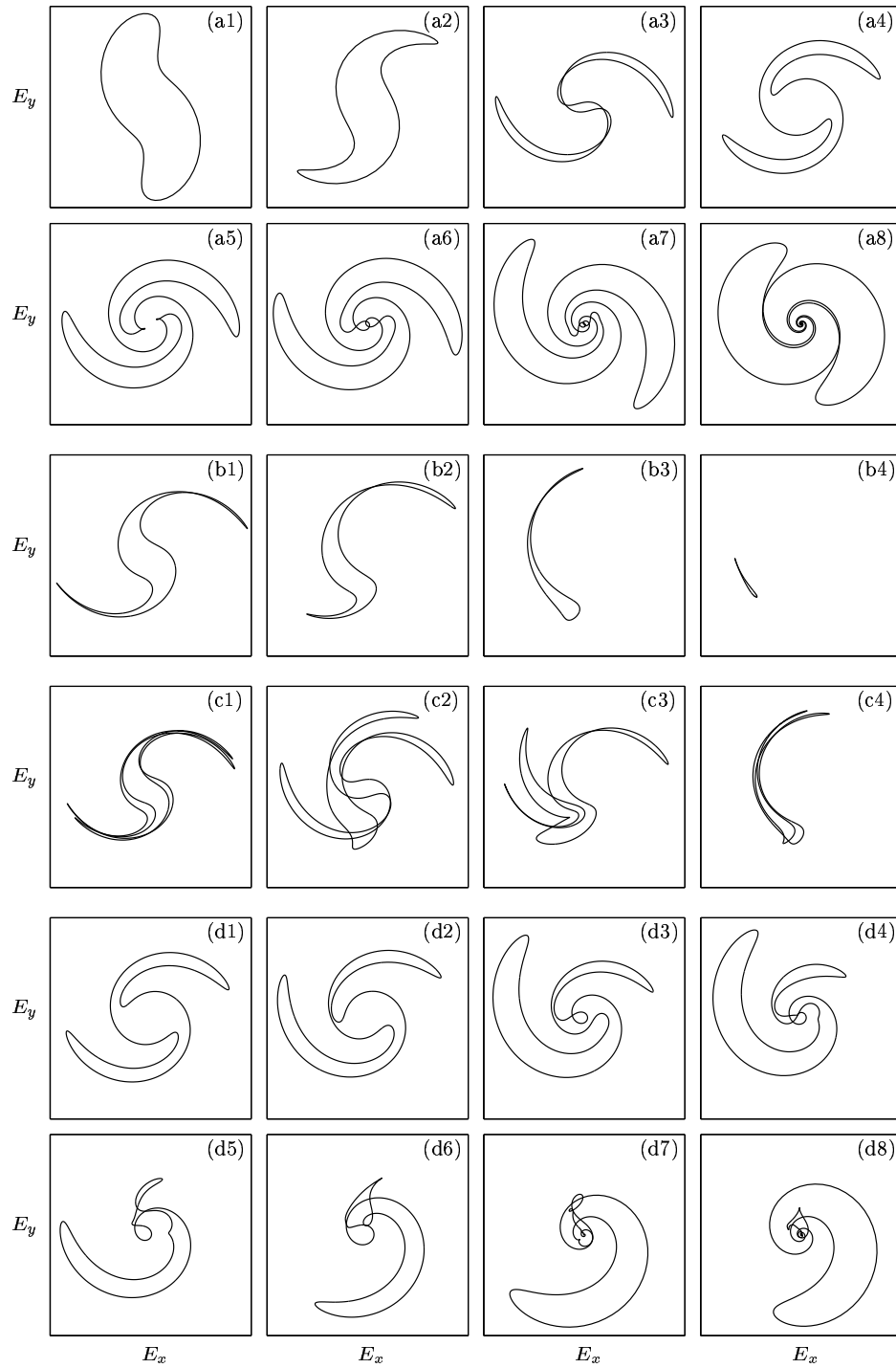


Figure 5: Phase portraits along the branches S_1 (a1)-(a8), N_1^1 (b1)-(b4), N_1^2 (c1)-(c4) and N_1^3 (d1)-(d8); shown in projection onto the E -plane. From (a1) to (a8) $\kappa\tau$ takes the values 2.0617, 1.9366, 1.1850, 0.4410, 0.9155, 0.7898, 0.4905 and 0.0973; from (b1) to (b4) $\kappa\tau$ takes the values 1.7929, 1.2871, 0.7964 and 0.7379; from (c1) to (c4) $\kappa\tau$ takes the values 1.7507, 1.1496, 1.3869 and 0.8458; and from (d1) to (d8) $\kappa\tau$ takes the values 0.4763, 0.7226, 0.9286, 1.3411, 1.6819, 1.5093, 2.1572 and 2.2414.

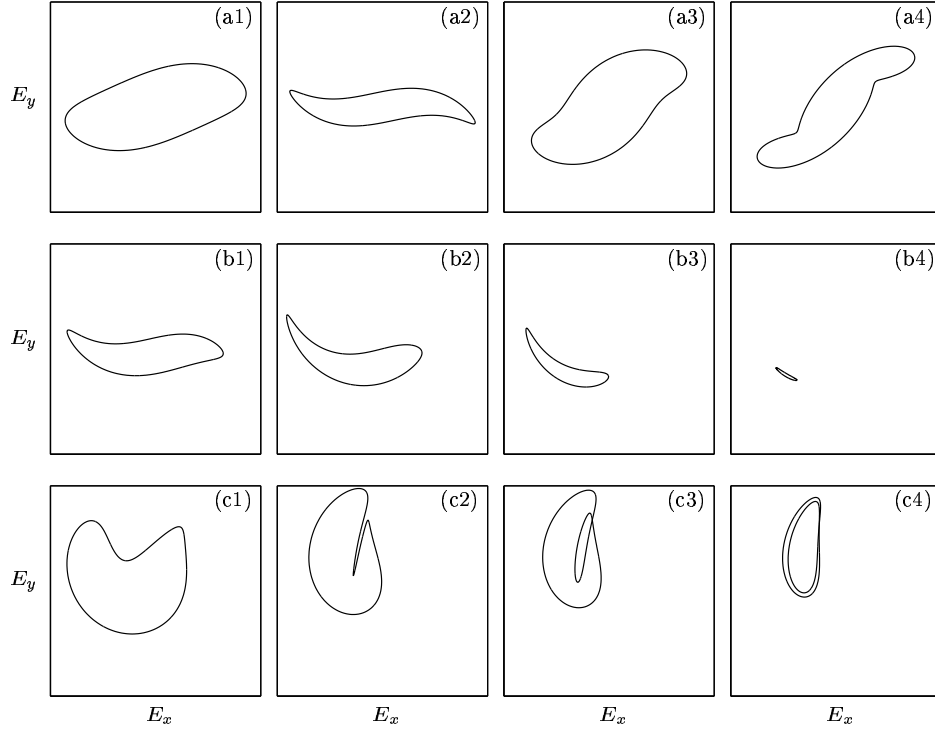


Figure 6: Phase portraits along the branches S_2 (a1)-(a4), N_2^2 (b1)-(b4) and N_2^3 (c1)-(c4); shown in projection onto the E -plane. From (a1) to (a4) $\kappa\tau$ takes the values 4.3221, 4.4738, 2.3500 and 6.6011; from (b1) to (b4) $\kappa\tau$ takes the values 4.2600, 3.3589, 1.5593 and 1.0411; and from (c1) to (c4) $\kappa\tau$ takes the values 2.3097, 3.6737, 4.0689 and 4.3529.

find other bifurcation scenarios. The dashed line in Figs. 4 (b) and (c) represents a period-doubling bifurcation connecting the branches N_2^3 and N_3^2 , and therefore, forms another connection between ECM2 and ECM3. Figure 6 (c1)–(c4) shows the development of the periodic orbit along N_2^3 . It is clearly seen to ‘fold’ over on itself, resulting in a period-two orbit in the local vicinity of the period-doubling bifurcation point, shown in panel (c4). This is a period-doubled version of the periodic orbit we find on N_3^2 , shown in Fig. 7 (c3). This connection is also clearly shown in Fig. 3 (a). The dashed box in Fig. 4 (c), enlarged in the inset, contains a hysteresis loop. Continuing ECM3 for decreasing $\kappa\tau$ shows that it is destabilized in a saddle-node bifurcation of limit cycles at $\kappa\tau \approx 6.703$. The solution then jumps to the non-symmetric branch N_3^1 which is stable up until a torus bifurcation at $\kappa\tau \approx 6.660$. However, starting from and continuing the stable periodic orbit on N_3^1 for increasing $\kappa\tau$ shows that it is destabilized in another torus bifur-

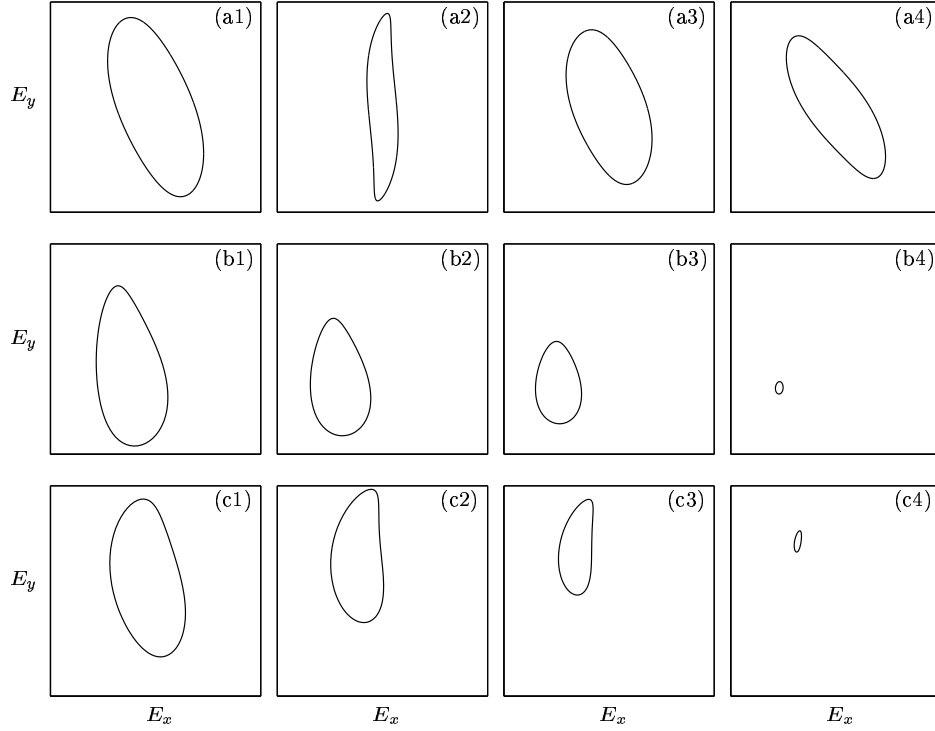


Figure 7: Phase portraits along the branches S_3 (a1)-(a4), N_3^1 (b1)-(b4) and N_3^2 (c1)-(c4); shown in projection onto the E -plane. From (a1) to (a4) $\kappa\tau$ takes the values 7.5033, 7.5696, 4.9669 and 7.3940; from (b1) to (b4) $\kappa\tau$ takes the values 6.6967, 6.6023, 6.5023 and 6.4098; and from (c1) to (c4) $\kappa\tau$ takes the values 5.0243, 4.6283, 4.3615 and 4.1800.

cation at $\kappa\tau \approx 6.707$. Simulation has shown that the ensuing torus is short lived and the solution jumps to ECM3 on S_3 . Thus, for $\kappa\tau \in [6.703, 6.707]$ one observes a region of bistability between the stable symmetric periodic orbit of S_3 and the stable non-symmetric periodic orbit of N_3^1 .

3.5 Homoclinic orbits

We now discuss in detail the homoclinic orbits identified in Fig. 3 (b), found at the end of the branches S_1 and N_1^3 , and at the end of the branch emanating from the Hopf bifurcation H_5 .

A routine allowing computation of connecting orbits using projection boundary conditions has been recently added to DDE-BIFTOOL [Samaey et. al. 2001]. A homoclinic orbit can be approximated by a very high period orbit, but by using projection boundary conditions one generally achieves a more accurate orbit, particularly if one then wants to follow it in

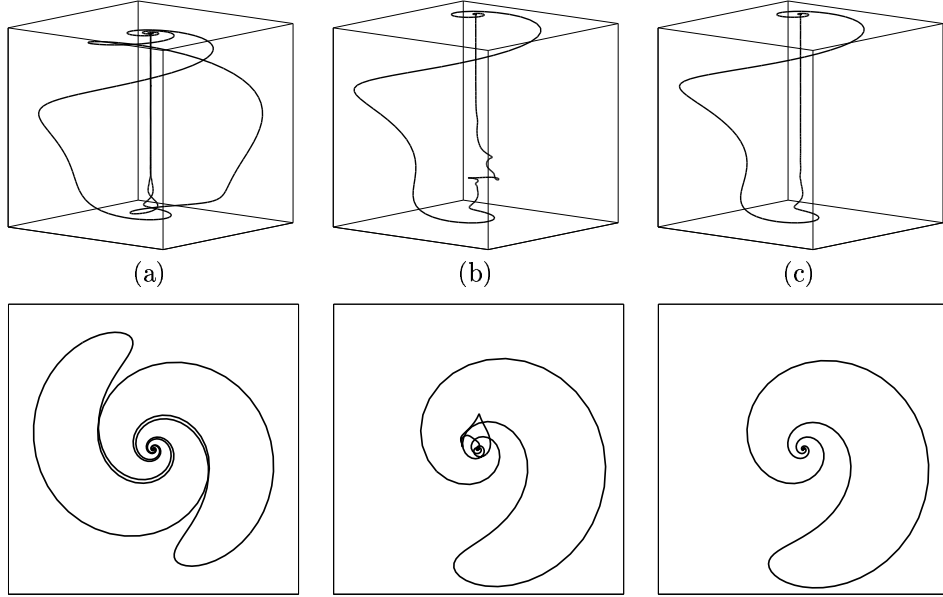


Figure 8: Homoclinic orbits of at the end of branches S_1 (a), N_1^3 (b) and the branch emanating from H_5 (c), shown in projection onto (E, N) -space and onto the E -plane respectively; the box is $[-800, 800] \times [-800, 800] \times [7.45 \times 10^8, 8.10 \times 10^8]$ and the square is $[-1000, 1000] \times [-1000, 1000]$.

parameters. This routine also gives stability information of the associated saddle steady states (or homoclinic points). In Sec. 3.4, we identified two possible homoclinic orbits of branches S_1 and N_1^3 , where the period of the orbit started to increase rapidly for small changes in $\kappa\tau$. It was shown in Figs. 5 (a1)–(a8) and (d1)–(d8) that both periodic orbits develop in a similar fashion, until finally the symmetric orbit, shown in panel (a8), appears as an image of the non-symmetric orbit, shown in panel (d8), together with its symmetric counterpart. We also identified a homoclinic orbit at the end of the branch emanating from the Hopf bifurcation H_5 .

All three homoclinic orbits are shown in Fig. 8. The saddle point involved in the homoclinic orbit in each case is the trivial saddle steady state at $(Re(E), Im(E), N) = (0, 0, 813.75)$. This trivial equilibrium does not depend on $\kappa\tau$. This was confirmed with DDE-BIFTOOL, which also gives stability information about the saddle point involved in the bifurcation. For all orbits, this saddle point has a leading real eigenvalue $\lambda_1 \approx -0.333$ and a complex conjugate pair of unstable eigenvalues $\lambda_{2,3} \approx 19.6 \pm i 58.9$. In all cases, this corresponds to the approximate one-dimensional attraction of

the trajectory towards the homoclinic point, along its stable manifold, and the two-dimensional spiral from the homoclinic point, along its unstable manifold, shown in Fig. 8.

The upper row of Fig. 8 shows the homoclinic orbits at the end of the symmetric branch S_1 (a), the non-symmetric branch N_1^3 (b) and the branch emanating from the Hopf bifurcation H_5 (c) in projection onto (E, N) -space. The lower row shows the same orbits projected onto the E -plane. All orbits shown were converted from high period to homoclinic orbits using the new DDE-BIFTOOL routine. However, there are still difficulties with convergence of the Newton iteration. It can clearly be seen that the non-symmetric homoclinic orbit in column (c) is exactly ‘one half’ of the homoclinic orbit in column (a). The remainder of the retracting ‘arm’ detailed in Sec. 3.4 can be seen in column (b). Investigations show that this ‘arm’ is not a numerical artifact. In fact, we were able to obtain convergence of the Newton iteration to this homoclinic orbit, so that it can be continued in two parameters.

Preliminary investigations using a 2-parameter continuation of the non-symmetric steady state, identified in Sec. 3.2, has revealed a T-point bifurcation [Glendinning and Sparrow 1986]. More specifically, this codimension two bifurcation occurs when a heteroclinic connection between the two non-symmetric equilibrium, detailed in [Green et. al. 2002], collides with the trivial saddle steady state. The existence of a T-point bifurcation implies the existence of a logarithmic spiral of homoclinic orbits associated with the trivial steady state. It is an organising centre of heteroclinic and homoclinic orbits. In fact, the two-dimensional unstable manifold of the trivial saddle steady state appears to form an upper organising boundary for the dynamics of the PCF laser. A full analysis of the T-point bifurcation is ongoing and beyond the scope of this paper.

4 Conclusions

We investigated periodic orbits in the PCF laser using recently developed continuation techniques. Stable symmetric periodic orbits corresponding to ECMs of the PCF laser have been shown to exist at different frequency ranges. Moreover, by continuing unstable periodic orbits we have provided a complete picture of how the ECMs of the PCF laser are connected to one another. We showed how bifurcating branches of non-symmetric periodic orbits ended in Hopf bifurcations. In each case, the respective Hopf point was shown to be associated with the same non-symmetric steady state and, therefore, a connection between the different ECMs of the PCF laser was found.

We identified all bifurcations of periodic orbits along the branches and key bifurcations were explained with phase portraits. This included a period-doubling bifurcation between two branches associated with different ECMs.

A bistability between a symmetric periodic orbit and non-symmetric periodic orbits leading to a hysteresis loop was identified. Furthermore, some branches were shown to end in homoclinic bifurcations associated with the trivial steady state of the PCF laser.

This investigation made use of the latest techniques in the bifurcation analysis of DDEs. In particular, we used very recent additions to DDE-BIFTOOL for the computation of homoclinic orbits and branch-switching at symmetry-breaking bifurcations. Our investigations of the PCF laser also show the use of these new techniques in general for DDEs arising in applications.

Future work will include analysing the homoclinic orbits in further detail, especially with respect to their symmetry properties and the T-point bifurcation. We will also investigate the sudden transitions from the periodic solutions to chaos with new tools, namely by computing unstable manifolds of saddle periodic orbits. One such sudden transition is the saddle-node bifurcation of limit cycles between ECM2 and the second bubble of chaos. It appears to involve chaotic transients and our aim is to find the chaotic saddle associated with this transition by computing the one-dimensional unstable manifold of the bifurcating saddle periodic orbit.

Acknowledgements

The authors thank Koen Engelborghs for his help with DDE-BIFTOOL and for implementing the routine allowing branch switching at symmetry-breaking bifurcations.

References

- Agrawal G. P. & Gray G. R. [1992] “Effect of phase-conjugate feedback on the noise characteristics of semiconductor lasers,” *Phys. Rev. A* **46**, 5890.
- Breton C. N., Tetu M. & Theriault S. [1991] “Laser-diode frequency control by resonant phase-conjugate reflection from an atomic vapor,” *Opt. Lett.* **16**, 1298.
- Diekmann O., Van Gils S. A., Lunel S. M. V. & Walther H. O. [1995] *Delay Equations: Functional-, Complex-, and Nonlinear Analysis* Springer-Verlag.
- Doedel E., Fairgrieve T., Sandstede B., Champneys A., Kuznetsov Y. & Wang X. [1997] *AUTO 97: Continuation and bifurcation software for ordinary differential equations*. <http://indy.cs.concordia.ca/auto/main.html>.

- Engelborghs K. [2000] “DDE-BIFTOOL: a Matlab package for bifurcation analysis of delay differential equations,” Technical Report TW-305 Department of Computer Science, K. U. Leuven, Belgium. <http://www.cs.kuleuven.ac.be/~koen/delay/ddebiftool.shtml>.
- Epstein I. R. & Pojman J. A. [1998] *An Introduction to Non-linear Chemical Oscillations* Oxford University Press, New York.
- Glendinning P. & Sparrow C. [1986] “T-points: A codimension two heteroclinic bifurcation,” *Journal of Statistical Physics* **43**, 479.
- Gray G. R., Huang D. & Agrawal G. P. [1994] “Chaotic dynamics of semiconductor lasers with phase-conjugate feedback,” *Phys. Rev. A* **49**, 2096.
- Green K. & Krauskopf B. [2001] “Global bifurcations and bistability at the locking boundaries of a semiconductor laser with phase-conjugate feedback,” Technical Report 2001.13 Applied Nonlinear Mathematics, University of Bristol, UK. <http://www.enm.bris.ac.uk/anm/preprints/2001r13.html>.
- Green K., Krauskopf B. & Engelborghs K. [2002] “Bistability and boundary crisis at the locking boundaries of a semiconductor laser with phase-conjugate feedback,” Technical Report 2002.02 Applied Nonlinear Mathematics, University of Bristol, UK. <http://www.enm.bris.ac.uk/anm/preprints/2002r02.html>.
- Haegeman B., Engelborghs K., Roose D., Pieroux D. & Erneux T. [2002] “Rupture of bifurcation bridges in semiconductor lasers subject to optical feedback,” Preprint, Department of Computer Science, K. U. Leuven, Belgium.
- Hale J. K. & Verduyn Lunel S. M. [1993] *Introduction to Functional Differential Equations* Springer-Verlag.
- Krauskopf B. & Green K. [2002] “Computing unstable manifolds in delay differential equations,” Technical Report 2002.01 Applied Nonlinear Mathematics, University of Bristol, UK. <http://www.enm.bris.ac.uk/anm/preprints/2002r01.html>.
- Krauskopf B. & Lenstra D., eds [2000] *Fundamental Issues of Nonlinear Laser Dynamics* Vol. 548 AIP Conference Proceedings.
- Krauskopf B., Gray G. R. & Lenstra D. [1998] “Semiconductor laser with phase-conjugate feedback: Dynamics and bifurcations,” *Phys. Rev. E* **58**, 7190.
- Krauskopf B., Van Tartwijk G. H. M. & Gray G. R. [2000] “Symmetry properties of lasers subject to optical feedback,” *Opt. Commun.* **177**, 347.

- Kuznetsov Y. [1995] *Elements of Applied Bifurcation Theory* Springer, Berlin.
- Longtin A., Milton J. G., Bos J. E. & Mackey M. C. [1990] "Noise and critical behavior of the pupil light reflex at oscillation onset," *Phys. Rev. A* **41**(12), 6992.
- Murray J. D. [1980] *Mathematical Biology* Vol. 19 Springer-Verlag, Berlin.
- Pieroux D., Erneux T., Haegeman B., Engelborghs K. & Roose D. [2001] "Bridges of periodic solutions and tori in semiconductor lasers subject to delay," *Phys. Rev. Lett.* **87**(193901).
- Pieroux D., Erneux T., Luzyanina T. & Engelborghs K. [2001] "Interacting pairs of periodic solutions lead to tori in lasers subject to delayed feedback," *Phys. Rev. E* **63**(036211).
- Samaey G., Engelborghs K. & Roose D. [2001] "Numerical computation of connecting orbits in delay differential equations," Technical Report TW-329 Department of Computer Science, K. U. Leuven, Belgium.
- Sciamanna M., Erneux T., Rogister F., Deparis O., Megret P. & Blondel M. [2002] "Bifurcation bridges between external-cavity modes lead to polarization self-modulation in vertical-cavity surface-emitting lasers," *Phys. Rev. A* **65**(041801(R)).
- Shimura T., Tamura M. & Kuroda K. [1993] "Injection locking and mode switching of a diode laser with a double phase-conjugate mirror," *Opt. Lett.* **18**, 1645.
- Van Tartwijk G. H. M. & Agrawal G. P. [1998] "Laser instabilities: a modern perspective," *Prog. Quantum Electron.* **22**, 43.
- Van Tartwijk G. H. M., Van der Linden H. J. C. & Lenstra D. [1995] "Theory of a diode laser with phase-conjugate feedback," *Opt. Lett.* **17**, 1590.
- Verduyn Lunel S. M. & Krauskopf B. [2000] "The mathematics of delay equations with an application to the Lang-Kobayashi equations," in Krauskopf and Lenstra (2000) pp. 66–86.